High-power sub-two-cycle mid-infrared pulses at 100 MHz repetition rate

I. Pupeza[1,2]*, D. Sánchez[2], J. Zhang[1,3], N. Lilienfein[1,4], M. Seidel[1,4], N. Karpowicz[1], T. Paasch-Colberg[4,5†], I. Znakovskaya[1,4], M. Pescher[4], W. Schweinberger[4,5], V. Pervak[4], E. Fill[1,4], O. Pronin[1,4], Z. Wei[3], F. Krausz[1,4], A. Apolonski[1,4] and J. Biegert[2,6]

Powerful coherent light with a spectrum spanning the mid-infrared (MIR) spectral range is crucial for a number of applications in natural as well as life sciences, but so far has only been available from large-scale synchrotron sources[1]. Here we present a compact apparatus that generates pulses with a sub-two-cycle duration and with an average power of 0.1 W and a spectral coverage of 6.8–16.4 µm (at −30 dB). The demonstrated source combines, for the first time in this spectral region, a high power, a high repetition rate and phase coherence. The MIR pulses emerge via difference-frequency generation (DFG) driven by the nonlinearly compressed pulses of a Kerr-lens mode-locked ytterbium-doped yttrium–aluminium–garnet (Yb:YAG) thin-disc oscillator. The resultant 100 MHz MIR pulse train is hundreds to thousands of times more powerful than state-of-the-art frequency combs that emit in this range[2–4], and offers a high dynamic range for spectroscopy in the molecular fingerprint region[4–7] and an ideal prerequisite for hyperspectral imaging[8] as well as for the time-domain coherent control of vibrational dynamics[9–11].

Over the past two decades, the development of coherent radiation sources in the MIR spectral region has been subject to intensive research. Most molecules exhibit fundamental vibrational modes in the range between 2 and 20 µm, which makes MIR spectroscopy a versatile tool for a variety of applications that range from fundamental science[10], over security and environmental applications (for example, the detection of weak gas traces[4–6]) to medical diagnostics[4,12]. For all the spectroscopy schemes, a spatially coherent, laser-like beam is highly desirable as a result of the increased brightness and the ability to focus tightly. Another essential parameter for spectroscopy experiments is the average power P of the source, because the signal-to-noise ratio (SNR) contributions of the detector noise and of the shot noise scale with P and $\sqrt{P}$, respectively[7]. Owing to the inferior noise figures of typical MIR detectors compared with visible detectors, a high spectral brightness is particularly important for MIR investigations. Finally, in the case of broadband pulsed radiation, the phase coherence of the pulses in combination with a repetition rate in the range of several tens of megahertz enables the resonant enhancement of the radiation in a passive optical cavity. This increases the interaction length with the investigated medium (for example, gas-phase volatile molecular components from living organisms) and, therefore, the sensitivity by a factor of $2FL/\pi$ (which can be of a few orders of magnitude), where F and L represent the cavity finesse and length,

respectively[4,5,13]. A radiation source that combines all these properties will also benefit other applications beyond molecular spectroscopy. Such a source, for instance, could be used as a strong, ultrashort bias to study and control ultrafast charge transport in dielectrics[9] or in semiconductors[10].

In the absence of suitable laser media, broadband coherent MIR sources rely on optical parametric processes to downconvert the frequency of ultrashort-pulsed, near-infrared (NIR) laser radiation[4,14]. In fact, recently parametric sources have enabled breakthroughs in many areas, including frequency comb spectroscopy[4,13,15], the generation of ultrahigh harmonics with kiloelectronvolt photon energies[16] and soft-X-ray absorption spectroscopy[17]. However, most of these sources employ oxide materials as nonlinear media, which are not transparent for wavelengths longer than ~5 µm (ref. 18). Non-oxide nonlinear crystals broadly transparent in the MIR typically suffer from unfavourable thermomechanical properties and (linear or nonlinear) absorption when pumped with NIR high-power sources[18]. In addition, generating radiation at increasingly long wavelengths suffers from an ever-more unfavourable photon-energy ratio between the pump and signal. Most of the state-of-the-art coherent sources in this spectral region are based on DFG in gallium selenide (GaSe), driven with wavelengths longer than 1 µm (refs 2,3,10). However, the driving laser sources either exhibit poor power scalability[2,3] or reach high pulse energies at the expense of a reduced repetition rate with a complex set-up[10]. Recent alternatives to DFG demonstrate supercontinuum generation (SCG) in chalcogenide fibres, driven by optical parametric amplifiers[19,20]. However, at wavelengths longer than 5 µm these sources produce average powers of a few milliwatts at best.

In this work, we present a source of coherent radiation that spans a spectrum from 6.8 to 16.4 µm (at −30 dB) and combines, for the first time, the desired properties of power scalability, high repetition rate (100 MHz) and phase coherence in this spectral region. The source is based on DFG driven by spectral components of the broadband NIR pulses of an Yb-based laser system in a chalcogenide crystal. Among the parametric processes, DFG allows for a convenient trade-off between efficiency and bandwidth[4]. In addition, the driving frequency components originate from one and the same pulse, so the carrier-envelope phase of the resulting pulses is inherently stabilized[4]. Furthermore, such a collinear intrapulse DFG exhibits the advantages of simplicity, compactness and reduced jitter[21,22]. In the prevailing context of coherent MIR sources, the power scalability in conjunction with a repetition rate

[1]Max-Planck-Institut für Quantenoptik, Hans-Kopfermann-Str. 1, Garching 85748, Germany. [2]ICFO - Institut de Ciencies Fotoniques, Barcelona Institute of Science and Technology, 08860 Castelldefels (Barcelona), Spain. [3]Beijing National Laboratory for Condensed Matter Physics and Institute of Physics, Chinese Academy of Sciences, Beijing 100190, China. [4]Fakultät für Physik, Ludwig-Maximilians-Universität München, Am Coulombwall 1, Garching 85748, Germany. [5]Department of Physics & Astronomy, King Saud University, PO Box 2455, Riyadh 11451, Saudi Arabia. [6]ICREA – Instituciò Catalana de Recerca i Estudis Avancats, Barcelona 08010, Spain. †Present addresses: TOPTICA Photonics AG, Lochhamer Schlag 19, Gräfelfing 82166, Germany. *e-mail: ioachim.pupeza@mpq.mpg.de
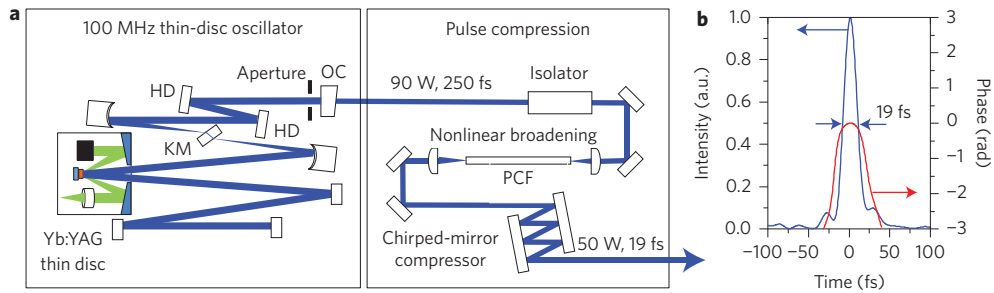
Figure 1 | Driving laser. a, Kerr-lens mode-locked Yb:YAG thin-disc oscillator. The 0.1 mm thin disc is wedged and curved with a radius of curvature of about 20 m. The disc is pumped at 940 nm in a multipass cavity configuration (green beam), which results in a pump spot diameter of 2.5 mm. The oscillator beam diameter on the disc is 2.2 mm ($1/e^2$ intensity). The 250 fs pulses (centre wavelength of 1,030 nm) produced by the oscillator are broadened to about 125 nm FWHM in an 80-mm-long large-mode-area PCF with a mode-field diameter of 35 µm. Temporal compression is subsequently achieved by 20 bounces on two types of chirped mirrors in a double-angle configuration, which accumulates a total group-delay dispersion of about –2,200 fs^2. The footprint of the oscillator and compression stage is 50×150 cm^2. HD, highly dispersive mirrors; OC, output coupler; KM, Kerr medium. **b**, Temporal intensity and phase of the compressed pulse measured by FROG (see Methods), which indicates a FWHM pulse duration of 19 fs.
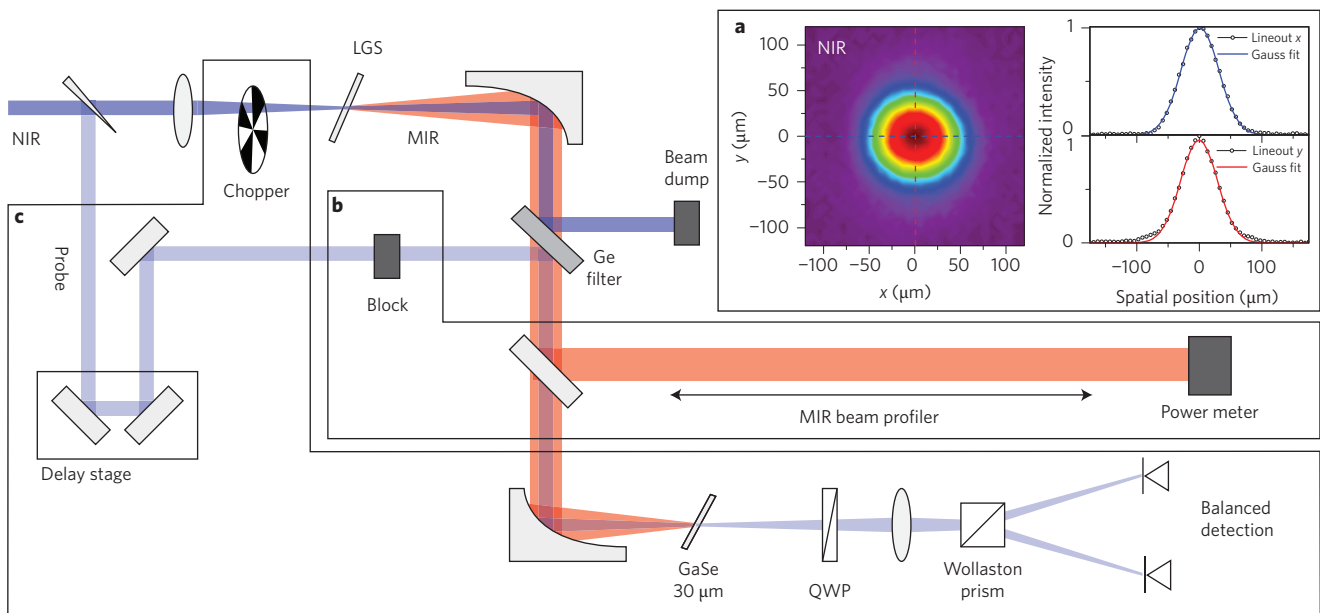

Figure 2 | MIR generation and detection set-up. The driving pulses are focused with a 250 mm focal-length lens onto the LGS crystal. **a**, The $1/e^2$ intensity diameter of the NIR focus is 130 µm, which leads to a peak intensity of 3.5×10^{11} W cm^{-2}. The NIR and MIR beams are collimated after the crystal with a 100 mm focal-length off-axis parabolic mirror. **b**, A 5 mm thick Ge filter reflects the NIR beam and transmits the MIR beam towards the diagnostics, thermal power meter and beam profiler (Fig. 3). **c**, EOS set-up. A low-power copy of the NIR pulse is obtained from a reflection off a thin fused-silica wedge in the main NIR beam path (and with negligible effect on the transmitted beam) and serves as the probe pulse for the EOS. The probe-pulse beam is combined collinearly with the MIR beam at the Ge filter and both beams are focused onto a 30-µm-thin GaSe crystal with a 100 mm focal-length off-axis parabolic mirror. The electric field of the MIR pulse modulates the birefringence of the crystal[10,25]. The NIR pulse probes the birefringence as a function of the delay between the two pulses, by a polarization-state detection scheme that consists of a quarter-wave plate (QWP), a Wollaston prism and a balanced detector using two Si photodiodes. The DFG-driving NIR beam is chopped at 2 kHz with a mechanical chopper, which enables lock-in detection. The measurements of the integrated power and of the beam profile are performed without the chopper.

of tens of megahertz is an essential aspect of our approach. To achieve this, the driving laser and nonlinear crystal choices were crucial and are discussed in the following.

The initial pulses are produced by a Kerr-lens mode-locked Yb:YAG thin-disc oscillator that operates at a 100 MHz repetition rate[23] (Fig. 1a). The oscillator delivers 250 fs pulses (full-width at half-maximum (FWHM)) with a carrier wavelength of 1,030 nm and an average power of 90 W. A temporal compression down to 19 fs with 50 W of average power is achieved in a nonlinear compression stage that consists of a photonic crystal fibre (PCF) followed by chirped mirrors[24] (Fig. 1b). Essential advantages of this driving source (for example, over state-of-the-art titanium–sapphire

systems[22], which produce similar pulse durations) include a high average power at the full repetition rate and the relatively low photon energy of 1.2 eV. The latter mitigates multiphoton absorption in the nonlinear crystal, which enables a high-power operation of the intrapulse DFG scheme.

Among the commercially available crystals, we found LiGaS$_2$ (LGS) to be the most suitable for power-scalable broadband DFG driven with the NIR source described above (Methods). At the available NIR average power and pulse duration we determined a damage threshold of 1×10^{12} W cm^{-2} peak intensity for LGS.

The experimental set-up for MIR generation is depicted in Fig. 2. The compressed pulses were focused into the LGS crystal such that
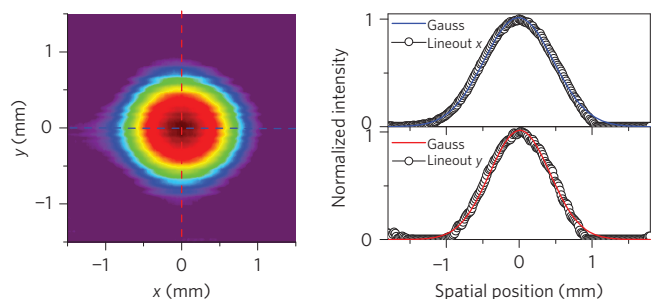
Figure 3 | MIR beam profile. The collimation of the MIR beam was achieved by adjusting the distance of the DFG focus to the collimating parabolic mirror and its orientation (Fig. 2). The profile of the MIR beam was measured with a microbolometer-array-based beam profiler. After achieving collimation, the MIR beam profile did not change notably along a few metres of propagation. The $1/e^2$ intensity diameter of the collimated beam is 1.897 mm in the horizontal (x) and 1.653 mm in the vertical (y) direction.

the peak intensity was a factor of about three below the damage threshold. This factor was chosen to avoid damage, given the spatial inhomogeneity of the crystal. The crystal was rotated such

that the impinging p-polarized laser light was distributed evenly between the extraordinary and the ordinary polarizations for type I phase matching. The generated MIR radiation propagated collinearly with the driving beam transmitted through the crystal. Both beams were collimated by an off-axis parabolic mirror and separated by a germanium filter. The duration of the driving NIR pulses is comparable to the half cycle of the carrier wave of the MIR pulses, which allows the direct electro-optical sampling (EOS)[10,25] of the oscillating MIR electric field (Methods). EOS provides direct access to the waveform of the MIR pulses and hence to their spectral amplitude and phase.

We used a 1 mm thick LGS crystal to generate MIR radiation via DFG. Figure 3 shows the MIR beam profile after collimation. The EOS trace is plotted in Fig. 4a along with the electric field of the MIR pulse, which was retrieved by deconvolution with the probe NIR pulse. The corresponding power spectral density (PSD) and spectral phase are plotted in Fig. 4b,c, respectively. The generated spectrum spans from 6.7 to 18 µm over a dynamic range of 2.7×10^4. The generated MIR power, directly after the LGS crystal, was 103 mW (Methods). The thickness of the Ge filter (5 mm) was chosen to compensate for the residual chirp of the MIR pulses. The intensity FWHM duration of the MIR pulse (determined from the processed time-domain trace) is 66 fs, which
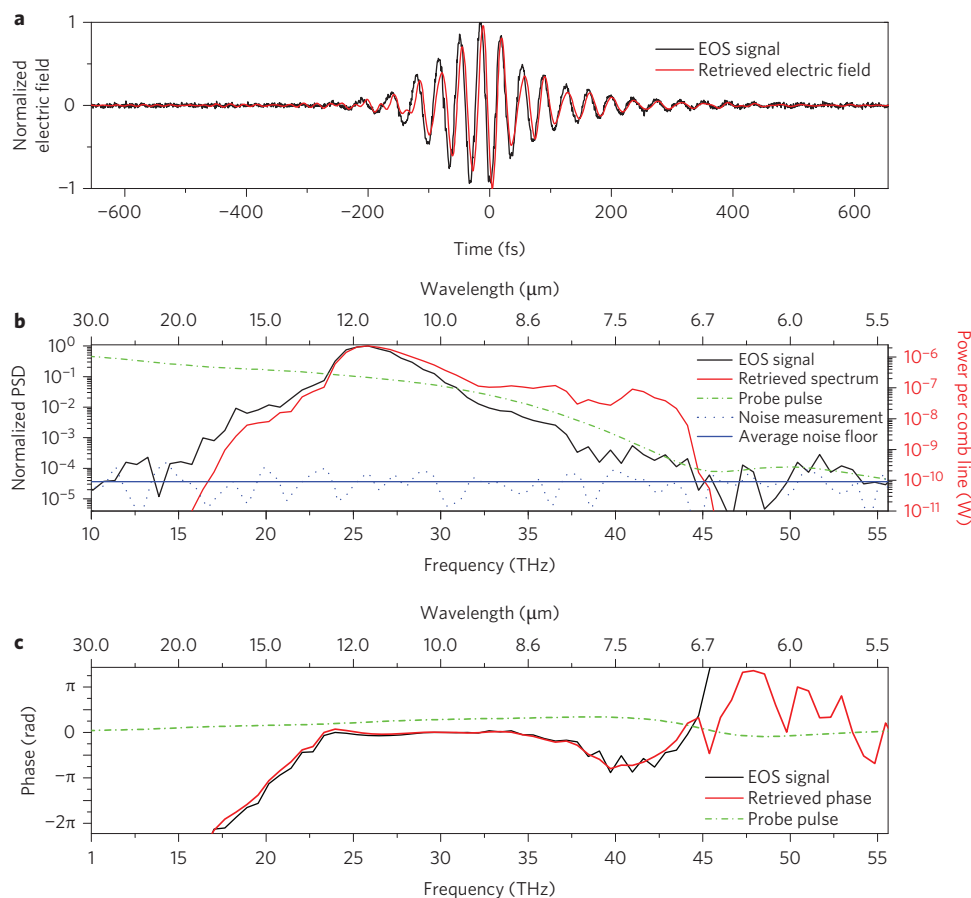

Figure 4 | DFG results. a, Raw EOS time-domain data (black line) of the MIR pulse consists of 3,000 measurement points with a lock-in integration time of 100 ms per point, which results in five minutes of measurement time. The SNR, determined in the time domain as the mean magnitude of the signal amplitude divided by the standard deviation of the peak signal, evaluated from several measurements, was 101. Retrieved MIR electric field data (red line) after deconvolution with the probe pulse (Methods). The FWHM of the intensity envelope is 66 fs. **b**, Normalized PSD of the Fourier transforms of the EOS time-domain trace, of the retrieved field and of the NIR probe pulse. The dynamic range of the measurement, determined as the peak of the signal PSD divided by the average detector noise floor (blue, continuous line), is 2.7×10^4. The absolute power per comb line of the generated MIR radiation, obtained by calibrating the normalized PSD of the retrieved MIR power spectrum by the independently measured total power and considering the pulse repetition frequency, is shown on the right axis. **c**, Spectral phase of the Fourier transforms of the EOS time-domain trace, of the retrieved field and of the NIR probe pulse. The spectral resolution of frequency-domain data is 0.64 THz.

corresponds to less than two cycles of the MIR electric field at the centre wavelength of 11.5 μm. The shortest MIR wavelength is generated by mixing the outer limits of the available NIR spectrum. Absorption data of the LGS crystal[26], as well as phase-matching simulations, indicate that towards long wavelengths the limitation of the generation process is given by the crystal absorption. The high dynamic range of the measurement confirms the expectation of phase coherence of the MIR pulse train that emerges via DFG. The source can be operated for several hours without any significant changes of the output power and of the spectrum.

In conclusion, we have demonstrated a compact broadband coherent MIR source of 100 MHz repetition-rate sub-two-cycle-duration pulses that spans the spectrum between 6.7 and 18 μm (at the cutoff), by driving DFG among the spectral components of the nonlinearly compressed pulses of a high-power Yb:YAG oscillator in LGS. To the best of our knowledge, in this spectral range the achieved average power per comb line is two-to-three orders of magnitude higher than those of state-of-the-art high-repetition-rate coherent sources[2–4]. The average power is the largest of any table-top source in this spectral region[10,19,20] and the spectral brightness of $\sim4.9 \times 10^{19}$ ph s^{-1} mm^{-2} sr^{-2} 0.1%BW^{-1} (ph, photons; sr, steradian; BW, bandwidth) at 11.5 μm (Methods) even exceeds that of large-scale facilities, such as the third-generation synchrotrons, by a few orders of magnitude[1]. The short duration of the driving NIR pulses enables EOS in this spectral range. This measurement confirms the pulse-to-pulse phase coherence of the MIR pulses, which is a first essential condition for employing this apparatus as a frequency comb in the future. As is known from the well-established technique of terahertz time-domain spectroscopy, the SNR in EOS can be shot-noise limited[25]. Thus, this work paves the way towards the ultimate combination of the advantages of resonant cavity enhancement with those of EOS, and so enable a new area of high-performance MIR spectroscopy. Furthermore, the temporally compressed few-cycle pulses pave the way for applications that require high intensities, such as further spectral broadening via SCG[19], new applications in ultrafast science[9–11] and nonlinear microscopy[8]. Further power scaling seems feasible by geometric scaling of the same approach[27] or by employing high-power chirped-pulse amplifiers[28].

Methods

Methods and any associated references are available in the online version of the paper.

References

1. Cinque, G., Frogley, M. D. & Bartolini, R. Far-IR/THz spectral characterization of the coherent synchrotron radiation emission at diamond IR beamline B22. *Rend. Fis. Acc. Lincei* **25** (suppl. 1), 33–47 (2011).
2. Gambetta, A. *et al.* Milliwatt-level frequency combs in the 8–14 μm range via difference frequency generation from an Er:fiber oscillator. *Opt. Lett.* **38**, 1155–1157 (2013).
3. Keilmann, F. & Amarie, S. Mid-infrared frequency comb spanning an octave based on an Er fiber laser and difference-frequency generation. *J. Infrared Millim. Te.* **33**, 479–484 (2012).
4. Schliesser, A., Picqué, N. & Hänsch, T. W. Mid-infrared frequency combs. *Nature Photon.* **6**, 440–449 (2012).
5. Adler, F., Thorpe, M. J., Cossel, K. C. & Ye, J. Cavity-enhanced direct frequency comb spectroscopy: technology and applications. *Annu. Rev. Anal. Chem.* **3**, 175–205 (2010).
6. Todd, M. W. *et al.* Application of mid-infrared cavity-ringdown spectroscopy to trace explosives vapor detection using a broadly tunable (6–8 μm) optical parametric oscillator. *Appl. Phys. B* **75**, 367 (2002).
7. Griffiths, P. R. & De Haseth, J. A. *Fourier Transform Infrared Spectrometry* 2nd edn (Wiley, 2007).
8. Dupont, S. *et al.* IR microscopy utilizing intense supercontinuum light source. *Opt. Express* **20**, 4887–4892 (2012).
9. Schiffrin, A. *et al.* Optical-field-induced current in dielectrics. *Nature* **493**, 70–74 (2013).
10. Schubert, O. *et al.* Sub-cycle control of terahertz high-harmonic generation by dynamical Bloch oscillations. *Nature Photon.* **8**, 119–123 (2014).
11. Krausz, F. & Stockman, M. I. Attosecond metrology: from electron capture to future signal processing. *Nature Photon.* **8**, 205–213 (2014).
12. Crosson, E. R. *et al.* Stable isotope ratios using cavity ring-down spectroscopy: determination of ^{13}C/^{12}C for carbon dioxide in human breath. *Anal. Chem.* **74**, 2003–2008 (2002).
13. Foltynowicz, A., Masłowski, P., Fleisher, A. J., Bjork, B. J. & Ye, J. Cavity-enhanced optical frequency comb spectroscopy in the mid-infrared application to trace detection of hydrogen peroxide. *Appl. Phys. B* **110**, 163–175 (2013).
14. Biegert, J., Bates, P. K. & Chalus, O. New mid-infrared light sources. *IEEE JSTQE* **18**, 521–540 (2012).
15. Meek, S. A., Poisson, A., Guelachvili, G., Hänsch, T. W. & Picqué, N. Fourier transform spectroscopy around 3 μm with a broad difference frequency comb. *Appl. Phys. B* **114**, 573–578 (2014).
16. Popmintchev, T. *et al.* Bright coherent ultrahigh harmonics in the keV X-ray regime from mid-infrared femtosecond lasers. *Science* **336**, 1287–1291 (2012).
17. Cousin, S. L. *et al.* High-flux table-top soft X-ray source driven by sub-2-cycle, CEP stable, 1.85-μm 1-kHz pulses for carbon K-edge spectroscopy. *Opt. Lett.* **39**, 5383–5386 (2014).
18. Petrov, V. Parametric down-conversion devices: the coverage of the mid-infrared spectral range by solid-state laser sources. *Opt. Mater.* **34**, 536–554 (2012).
19. Petersen, C. R. *et al.* Mid-infrared supercontinuum covering the 1.4–13.3 μm molecular fingerprint region using ultra-high NA chalcogenide step-index fibre. *Nature Photon.* **8**, 830–834 (2014).
20. Møller, U. *et al.* Multi-milliwatt mid-infrared supercontinuum generation in a suspended core chalcogenide fiber. *Opt. Express* **23**, 3282–3291 (2015).
21. Kaindl, R. A., Eickemeyer, F., Woerner, M. & Elsaesser, T. Broadband phase-matched difference frequency mixing of femtosecond pulses in GaSe: experiment and theory. *Appl. Phys. Lett.* **75**, 1060–1062 (1999).
22. Fattahi, H., Schwarz, A., Keiber, S. & Karpowicz, N. Efficient, octave-spanning difference-frequency generation using few-cycle pulses in simple collinear geometry. *Opt. Lett.* **38**, 4216–4219 (2013).
23. Zhang, J. *et al.* 260-megahertz, megawatt-level thin-disk oscillator. *Opt. Lett.* **40**, 1627–1630 (2015).
24. Pronin, O. *et al.* High-power multi-megahertz source of waveform-stabilised few-cycle light. *Nature Commun.* **6**, 6988 (2015).
25. Porer, M., Ménard, J.-M. & Huber, R. Shot noise reduced terahertz detection via spectrally postfiltered electro-optic sampling. *Opt. Lett.* **39**, 2435–2438 (2014).
26. Isaenko, L. *et al.* Growth and properties of LiGaX2 (X = S, Se, Te) single crystals for nonlinear optical applications in the mid-IR. *Cryst. Res. Technol.* **38**, 379–387 (2003).
27. Brons, J. *et al.* Energy scaling of Kerr-lens mode-locked thin-disk oscillators. *Opt. Lett.* **39**, 6442–6445 (2014).
28. Jocher, C., Eidam, T., Hädrich, S., Limpert, J. & Tünnermann, A. Sub 25 fs pulses from solid core nonlinear compression stage at 250 W of average power. *Opt. Lett.* **37**, 4407–4409 (2012).

Author contributions

I.P., D.S., J.Z., N.L., M.S., N.K., T.P., W.S., V.P., E.F., O.P., Z.W., F.K., A.A. and J.B. conceived and designed the experiments. I.P., D.S., J.Z., N.L., M.S., T.P., I.Z., M.P., W.S. and V.P. performed the experiments. I.P., D.S., N.L., M.S., N.K., T.P., I.Z. and W.S. analysed the data. I.P., D.S., J.Z., N.L., M.S., N.K., T.P., I.Z., V.P., E.F., O.P., Z.W., F.K., A.A. and J.B. contributed materials and/or analysis tools. I.P., D.S., J.Z., N.L., M.S., N.K., T.P., M.P., W.S., E.F., F.K., A.A. and J.B. wrote the paper.

Additional information

Supplementary information is available in the online version of the paper. Reprints and permissions information is available online at www.nature.com/reprints. Correspondence and requests for materials should be addressed to I.P.

Competing financial interests

The authors declare no competing financial interests.

Methods

Choice of the crystal. The nonlinear crystal employed for DFG must be transparent for both the driving NIR and the generated MIR spectra, in addition to exhibiting a high damage threshold and good thermal properties. To date there are only a few crystals that satisfy these requirements[18], namely $AgGaS_2$ (AGS), $LiInS_2$ (LIS), $LiInSe_2$, LGS, $LiGaSe_2$ and GaSe. We discarded GaSe and AgS because of their small bandgap ($\sim$500 nm) and, in the case of GaSe, high linear absorption[29]. With a full 3D nonlinear wave-propagation code[30] we simulated the DFG process to study the phase-matching properties of the remaining crystals. The results suggest that the broadest DFG spectra are generated in LGS and LIS in a type I phase-matching configuration in the xz plane of the crystals. We then conducted a preliminary experiment to test the laser-induced damage threshold (LIDT). By scanning the crystals along the optical axis towards a tight focus, we determined LIDTs of 0.5×10^{12} and 1×10^{12} W cm^{-2} for LIS and LGS, respectively, at a pulse duration of approximately 20 fs. However, we observed a spatial inhomogeneity of the crystals, which manifested itself in a variation of the LIDT by a factor of approximately three, the above-mentioned values being the maxima measured. Furthermore, the ratio of the number of 'good spots' to the number of 'bad spots' strongly depended on the crystal batch. These observations are in accordance with the involved manufacturing process[26], which is a commonality for non-oxide crystals, and results in defects and residual losses typically of at least one order of magnitude larger than those for the best oxide crystals[18]. The crystals used in this work were purchased from the company Ascut Ltd & Co. Provided that the beam traversed the crystal through a 'good spot', no long-term degradation was observed.

Measurement of the MIR average power. For power measurements the chopper wheel was removed. The wavelength dependence of the attenuation on transmission through the Ge filter (taking into account the Fresnel reflections at the interfaces with air) and reflection from three metallic mirrors between the crystal and the power meter is, in good approximation, constant in the range between 4 and 14 μm (where >99% of the generated power is located) and amounts to 29.5%. The Ge filter was placed in a water-cooled mount to avoid temperature-dependent refractive-index changes. The peak temperature of the filter was measured with a thermal camera and amounted to 37 °C. At this temperature, it can be assumed that the transmission of Ge is nearly the same as that at room temperature. To validate this assumption experimentally, we transmitted the MIR beam back through the Ge plate, in particular through the spot at which the NIR beam impinges on the plate (at a slight angle with respect to the incoming beam to enable a spatial separation). The measured transmission agreed excellently with the value predicted by calculations based on literature values. The power measured was 30.5 mW (which corresponds to 103 mW of generated MIR) and the accuracy of the measurement is approximately 10%. To make more MIR power available for experiments, the Ge plate that splits the collinear NIR and MIR beams after the DFG focus could, for example, be placed under Brewster's angle for the MIR radiation.

EOS detection. The EOS time-domain trace represents, in good approximation, a convolution of the MIR electric field, which linearly modulates the birefringence of the electro-optic GaSe crystal, with the intensity envelope of the NIR probe pulses. To retrieve the MIR electric field in the time domain, we carried out a deconvolution of the recorded trace with the intensity envelope of the probe pulse, determined from a frequency-resolved optical gating (FROG) measurement. This deconvolution was carried out in the frequency domain, after applying a super-Gaussian filter of order eight with the centre frequency of 30 THz and a bandwidth of $\sigma = 12$ THz to the raw data, corrected for the transmission of the Ge filter (data obtained from Thorlabs). This deconvolution is not necessary in linear reference-sample time-domain spectroscopy measurements. Owing to the slight wavelength dependence of the beam splitter used to split the EOS probe pulse from the main NIR beam, the probe pulse (dash-dot green line in Fig. 4b,c) has a slightly longer duration (22 fs, determined by FROG). The PSD of its intensity envelope rapidly decreases for wavelengths shorter than 7 μm, which indicates the detection limit of our set-up. Thus, the duration of 66 fs for the MIR pulse is an upper-bound estimation of the actual pulse duration.

Brightness estimation. From the PSD measured via EOS and the independently determined total power of 103 mW we infer a power of 1.1×10^{-4} W in 0.1% of the FWHM band around the central wavelength of $\lambda = 11.5$ μm, which corresponds to a photon flux of 6.4×10^{15} ph s^{-1} 0.1%BW^{-1}. Owing to the spatial coherence of the DFG process we assume that a diffraction-limited MIR beam emerges from the focus in the crystal with $w_0 = 65$ μm (Fig. 2a). This yields an area of 1.3×10^{-2} mm^2 and a divergence angle of $\lambda/(\pi w_0) = 56.3$ mrad, which corresponds to a solid angle of 0.01 sr. The resulting brightness is 4.9×10^{19} ph s^{-1} mm^{-2} sr^{-1} 0.1%BW^{-1}.

References

29. Nikogosyan, D. N. *Nonlinear Optical Crystals: A Complete Survey* (Springer, 2005).
30. Arisholm, G. General numerical methods for simulating second-order nonlinear interactions in birefringent media. *J. Opt. Soc. Am. B* **14,** 2543–2549 (1997).